Reduced graphene oxide wrapped Cu2O supported on C3N4: an efficient visible light responsive semiconductor photocatalyst.

GANESH BABU, S., VINOTH, R., SURYA NARAYANA, P., BAHNEMANN, D. and NEPPOLIAN, B.

2015

The supplementary material published alongside this article has been included at the end of the file.

Reduced graphene oxide wrapped Cu_2O supported on C_3N_4: An efficient visible light responsive semiconductor photocatalyst

S. Ganesh Babu,[1] R. Vinoth,[1] P. Surya Narayana,[1] Detlef Bahnemann,[2] and B. Neppolian[1,a]
[1]*SRM Research Institute, SRM University, Kattankulathur, Chennai 603203, India*
[2]*Institute of Technical Chemistry, Leibniz University of Hannover, D-30167 Hannover, Germany*

(Received 29 April 2015; accepted 26 July 2015; published online 25 August 2015)

Herein, Cu_2O spheres were prepared and encapsulated with reduced graphene oxide (rGO). The Cu_2O–rGO–C_3N_4 composite covered the whole solar spectrum with significant absorption intensity. rGO wrapped Cu_2O loading caused a red shift in the absorption with respect to considering the absorption of bare C_3N_4. The photoluminescence study confirms that rGO exploited as an electron transport layer at the interface of Cu_2O and C_3N_4 heterojunction. Utmost, ~2 fold synergistic effect was achieved with Cu_2O–rGO–C_3N_4 for the photocatalytic reduction of 4-nitrophenol to 4-aminophenol in comparison with Cu_2O–rGO and C_3N_4. The Cu_2O–rGO–C_3N_4 photocatalyst was reused for four times without loss in its activity. [http://dx.doi.org/10.1063/1.4928286]

Semiconductor photocatalysis technique is one of the best environmental friendly methods for the degradation of organic pollutants, removal of heavy metals, water purification, and disinfection.[1–3] Owing to the non-toxicity, chemical stability, insolubility in water, and the favorable optical property, titania (TiO_2) is regarded as the promising material to approach the universal energy and environmental crises.[4,5] Unfortunately, TiO_2 can only be excited by ultraviolet (UV) light, which limits its application to a great extend.[6] Many approaches have been proposed to make the TiO_2 as visible light active: metal ion implanted TiO_2, reduced TiO_x photocatalysts, non-metal doped TiO_2, composites of TiO_2 with semiconductor having lower band gap energy, sensitizing of TiO_2 with dyes, and TiO_2 with luminescence agent.[7–12] On the other hand, a great research effort is being taken to replace the UV light active TiO_2 photocatalyst with the visible light active stable photocatalysts. Recently, Wang *et al.* reported a novel metal free polymer material and graphitic carbon nitride (g-C_3N_4) for the production of H_2 by splitting of water via photocatalysis.[13] Because of its lower band gap energy, g-C_3N_4 (E_g = 2.7 eV) can absorb natural sunlight and thereby active under visible light. More interestingly, C_3N_4 possesses more favorable properties to be a suitable photocatalyst such as extremely thermally stable, chemically inert, and resistive towards photocorrosion.[14] High recombination rate of electron-hole pairs makes the pristine C_3N_4 to be less efficient under visible light irradiation that limits its energy and environmental applications. Furthermore, C_3N_4 suffers with inadequate photon absorption capability after ~460 nm.[15] Many methods have been developed to overcome the above two demerits such as doping of metals or non-metals and combining with graphene.[16,17] Hence, to make the C_3N_4 photocatalyst more efficient, copper(I) oxide (Cu_2O) is deposited on the surface of C_3N_4. It is well known that Cu_2O is a promising visible light active photocatalyst due to its low band gap energy (2.2 eV), nontoxicity, and natural abundance.[18] For example, Tion *et al.* reported the preparation of C_3N_4/Cu_2O heterojunction and its photocatalytic studies for the degradation of methyl orange dye under visible light irradiation.[19]

[a]Author to whom correspondence should be addressed. Electronic mail: neppolian.b@res.srmuniv.ac.in

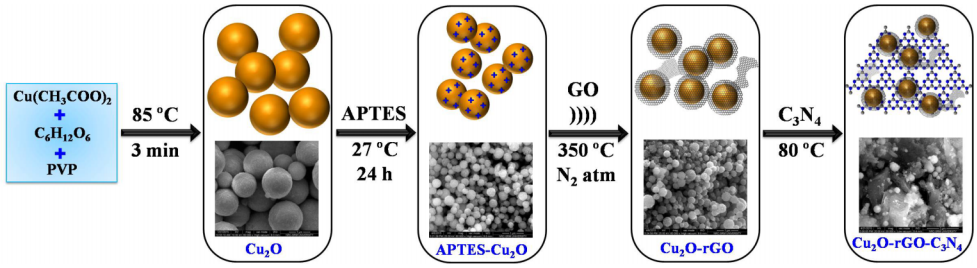

FIG. 1. Schematic illustration for the preparation of Cu_2O–rGO–C_3N_4 photocatalyst.

To enhance the reactivity of the photocatalyst or to reduce the charged carrier recombination, rGO was used as a potential carbonaceous solid support in many of the photocatalytic systems.[20] But insertion of the rGO exactly at the interfacial of the two heterojunction is another key challenge. Hence, in this particular research work, Cu_2O spheres were wrapped with rGO layer and then deposited on the surface of C_3N_4, so that the rGO layers are precisely in between the p-n heterojunction of Cu_2O and C_3N_4. So, rGO effectively increased the charged carrier mobility in the interfacial region of the two semiconducting materials. To prove the efficacy of the prepared composite, photocatalytic reduction of 4-nitrophenol was performed under visible light irradiation which is an important organic reaction as per industrial perspective.

The schematic representation for the preparation of Cu_2O–rGO–C_3N_4 photocatalyst is illustrated in Figure 1. Cu_2O spheres were prepared by simple wet solution method using $Cu(CH_3COO)_2 \cdot H_2O$, glucose, and polyvinyl pyrolidone. The as-prepared Cu_2O spheres were characterized by scanning electron microscope - energy dispersive spectroscopy (SEM-EDS) analysis. As depicted in Figure 2(a), the Cu_2O possesses exact spherical in shape. This hierarchical spherical structure made the wrapping of rGO extremely straightforward. More importantly, no defective spots were identified in the spherical structure which emphasized the reliability of this preparation protocol [Figures 2(b)-2(d)]. Furthermore, the purity of the sample was estimated by EDS analysis which confirmed the presence of Cu and O (the elemental C peak came from double side carbon tape used as a sample holder for SEM-EDS measurements) [Figure 2(e)]. In order to find the phase purity of the prepared Cu_2O spheres, XRD analysis was carried out and the pattern exactly resembled the XRD pattern of Cu_2O (JCPDS card number is 77-0199).[21] More importantly, no peaks were observed with respect to the CuO, which confirmed the complete reduction of Cu^{2+} ($Cu(CH_3COO)_2 \cdot H_2O$) to Cu^{+} (Cu_2O) [Figure 2(f)].[22]

XRD patterns of Cu_2O, (3-Aminopropyl)triethoxysilane (APTES) modified Cu_2O, Cu_2O–rGO, Cu_2O–rGO–C_3N_4 and C_3N_4 are depicted in Figure 3. As discussed previously, the XRD peaks of phase pure primitive lattice Cu_2O spheres were observed. The XRD pattern of surface modified Cu_2O using APTES precisely resembled with the pure Cu_2O spheres that revealed that surface modification only generated positive charges on the surface of Cu_2O spheres but not created any changes in the phases and oxidation states. However, while wrapping the rGO layer onto the surface of Cu_2O spheres, a new XRD peak centered at $2\theta = 38.74°$ was appeared, corresponding to the (111) plane of CuO.[23,24] This oxidation of Cu_2O to CuO occurred during the calcination process. Nevertheless, the intensity of the peak was very less which authenticated that the over-oxidation was very minimal because the calcination performed under inert condition (in presence of N_2 atmosphere). It is worth to mention here that no authenticated peaks were observed for rGO in the XRD spectra of both Cu_2O–rGO and Cu_2O–rGO–C_3N_4 photocatalysts which might be due to the lowest loading of GO (1%). The additional two peaks in the XRD pattern of Cu_2O–rGO–C_3N_4 photocatalyst at 13.05° and 27.55° were corresponded to the (001) and (002) planes of graphitic C_3N_4 (g-C_3N_4), respectively.[25] This was further confirmed by comparing the XRD spectrum of bare g-C_3N_4 as shown in Figure 3.

Figure 4 represents the SEM images of APTES modified Cu_2O, Cu_2O–rGO and Cu_2O–rGO–C_3N_4 photocatalysts. It is seen that APTES not only created positive charges on the surface of Cu_2O spheres but also reduced the particle size which is clearly evident from the SEM images of

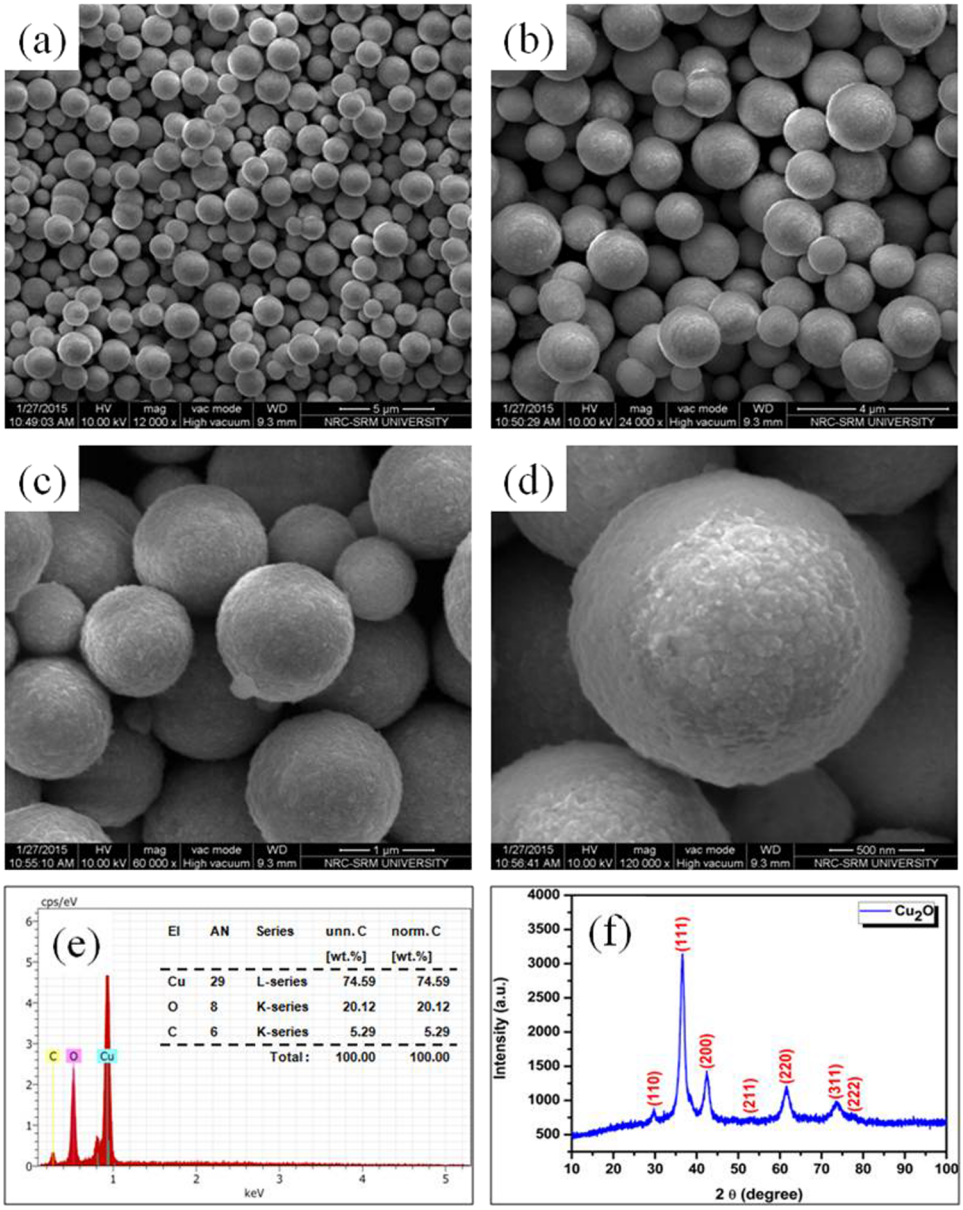

FIG. 2. (a)-(d) SEM images of hierarchically structured Cu_2O spheres with different magnifications. (e) EDX graph [inset: elemental wt. % table] and (f) XRD pattern of Cu_2O spheres.

APTES modified Cu_2O [Figures 4(a) and 4(b)]. This size contraction might be due to the existence of more positive charges on the surface of Cu_2O. Presence of rGO layer in Cu_2O–rGO photocatalyst was verified by the SEM images as shown in Figure 4(c). Complete wrapping of rGO over Cu_2O spheres were confirmed from the Figure 4(d). Nonetheless, only a meager amount of free rGO layers were identified at the background which authenticated the complete utilization of rGO for the wrapping of Cu_2O spheres.[26] The SEM images of Cu_2O-rGO-C_3N_4 composite are depicted in Figures 4(e) and 4(f). In addition, even after introducing C_3N_4, the spherical morphology of Cu_2O was maintained. Furthermore, the SEM results revealed that the rGO wrapped Cu_2O spheres were dispersed homogeneously on the surface of C_3N_4.

In order to understand the absorption behavior and band gap of Cu_2O, C_3N_4 and Cu_2O–rGO–C_3N_4, ultraviolet-visible (UV-vis) spectroscopy was studied in diffused reflectance spectroscopy (DRS) mode. The results are shown in Figure 5. The absorption range was restricted to 460 and

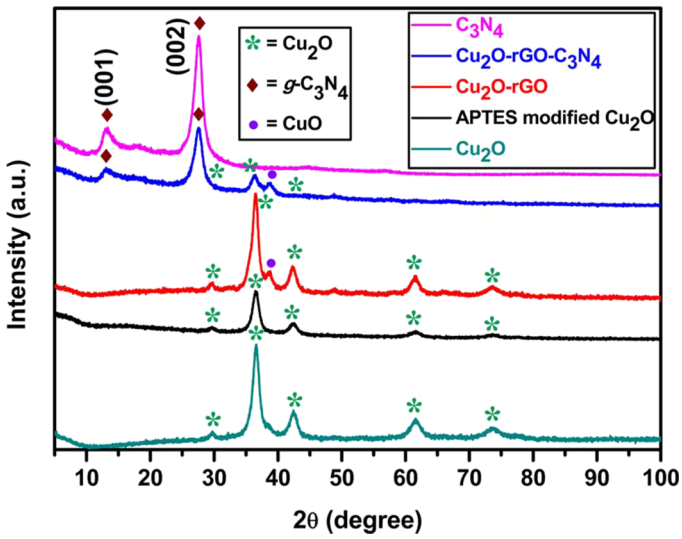

FIG. 3. XRD patterns of Cu_2O, APTES modified Cu_2O, Cu_2O–rGO, Cu_2O–rGO–C_3N_4, and C_3N_4.

600 nm for pristine Cu_2O and C_3N_4, respectively, which was in good agreement with the literature reports.[27,28] But the Cu_2O–rGO–C_3N_4 composite covered almost the whole solar spectrum that favors the material to be photoactive [Figure S1(a) in the supplementary material].[36] The absorption intensity was also remarkably increased after loading Cu_2O–rGO to C_3N_4 and appeared as a red shift in comparison with bare C_3N_4. The adsorption edge of pristine C_3N_4 was 450 nm which can be assigned to the band gap energy of 2.75 eV [Figure S1(b) in the supplementary material].[36] Bare Cu_2O possesses the band gap energy of 2.20 eV [Figure S1(c) in the supplementary material].[36] Similarly, the absorption edge of Cu_2O–rGO–C_3N_4 photocatalyst was about 477 nm and the calculated band gap was 2.60 eV [Figure S1(d) in the supplementary material].[29,36]

Photoluminesence (PL) spectroscopy is one of the powerful tools to examine the charge transfer, migration, and extend of separation in photocatalysts. Figure 5 shows the PL spectra of pure C_3N_4, Cu_2O, Cu_2O–rGO, and Cu_2O–rGO–C_3N_4 photocatalysts. In the PL spectrum of pristine C_3N_4, a peak centered at 450 nm, corresponding to the band gap of C_3N_4.[29] The other three materials, namely, Cu_2O, Cu_2O–rGO, and Cu_2O–rGO–C_3N_4 showed broad PL emission peak from 500 to 700 nm. Very importantly, the peak intensity at this region was in the order of Cu_2O > Cu_2O–rGO > Cu_2O–rGO–C_3N_4 which confirmed that the charged carriers recombination was very high in pristine Cu_2O. It is well known fact that rGO has higher carrier mobility and thereby reduced the recombination rate in Cu_2O–rGO photocatalyst. As a result, the peak intensity was lesser for Cu_2O–rGO than bare Cu_2O. But the peak intensity was decreased further by adding C_3N_4 to Cu_2O–rGO. It is worth to mention here that the Cu_2O–rGO–C_3N_4 photocatalyst showed two PL emission peaks at around 500 to 700 nm and 450 nm which were emerged because of Cu_2O and C_3N_4, respectively. Astonishingly, both the emission peaks were suppressed that inferred that the recombination of charged carriers was completely prevented.

All the characterization techniques results, especially the optical studies (UV-vis DRS and PL), indicate that Cu_2O–rGO–C_3N_4 can be a very good material for visible light active photocatalytic reactions. Therefore, photocatalytic reduction of 4-nitrophenol to 4-aminophenol was performed in presence of Cu_2O–rGO–C_3N_4 photocatalyst under visible light irradiation. For comparison, the photocatalytic reduction of 4-nitrophenol was performed using bare Cu_2O, rGO wrapped Cu_2O, pure C_3N_4, Cu_2O–C_3N_4, and Cu_2O–rGO–C_3N_4 (Figure 6). Among the photocatalysts used, bare Cu_2O showed lesser activity whereas the rGO wrapping increased the photocatalytic reduction property of Cu_2O. But the activity was comparatively lesser than the photocatalytic reduction of 4-nitrophenol using pristine C_3N_4. The photocatalytic activity of pristine C_3N_4 was increased slightly by loading bare Cu_2O (without rGO) spheres. However, the Cu_2O–rGO–C_3N_4 composite exhibited maximum reduction of 4-nitrophenol. This can be well explained by the fact that the recombination rate was

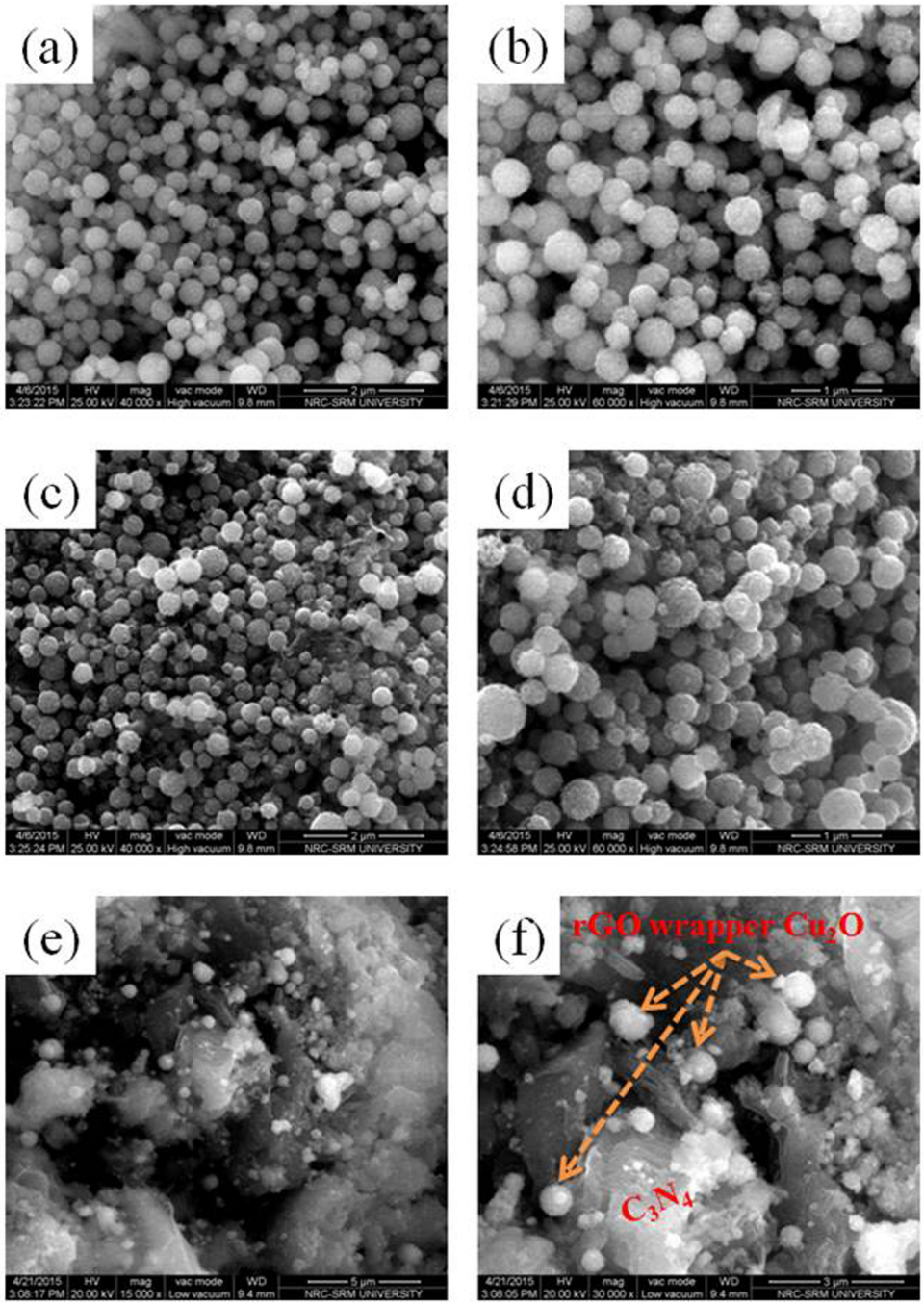

FIG. 4. SEM images of (a) and (b) APTES modified Cu_2O (c) and (d), rGO wrapped Cu_2O, and (e) and (f) Cu_2O–rGO–C_3N_4 composites.

completely prevented in Cu_2O–rGO–C_3N_4 photocatalyst as evident by the PL studies (Figure 5) and also that it possessed utmost visible light absorption capability as supported by the UV-vis DRS absorption spectrum [Figure S1(a) in the supplementary material].[36]

Based on the results, a tentative mechanism was proposed for the photocatalytic reduction of 4-nitrophenol using Cu_2O–rGO–C_3N_4 photocatalyst in presence of sodium sulfite under visible light irradiation (Figure 7). Both Cu_2O and C_3N_4 are visible light active photocatalysts and hence electron-hole pairs were generated in both the catalysts under visible light irradiation. The conduction band (CB) and valance band (VB) energy levels of Cu_2O are −0.7 V and 1.3 V, respectively.[30]

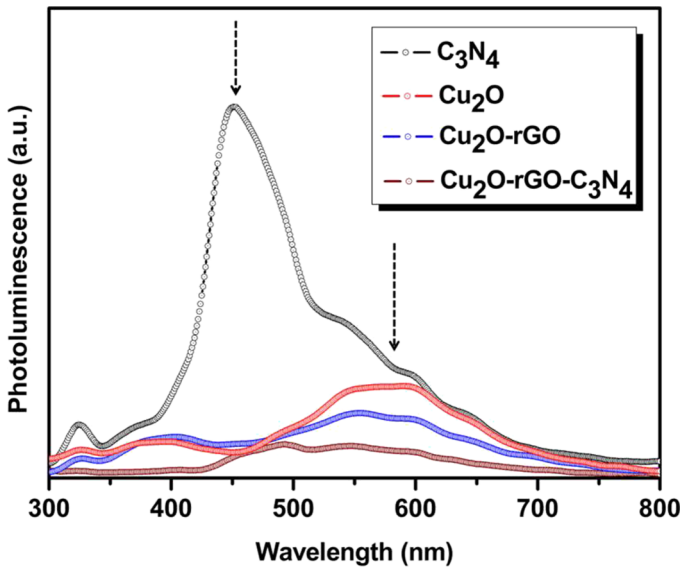

FIG. 5. Photoluminescence spectra of C_3N_4, Cu_2O, Cu_2O–rGO, and Cu_2O–rGO–C_3N_4 photocatalysts.

Since Cu_2O is a p-type semiconductor, the Fermi level energy is close to the VB.[31] On the other hand, the CB and VB potential of C_3N_4 are −1.13 V and 1.57 V, respectively.[32] But the Fermi level is nearer to the CB because it is an n-type semiconductor.[33] Apparently, the band structure of Cu_2O and C_3N_4 is not suitable for the formation of heterojunction. Nevertheless, when the rGO wrapped Cu_2O deposited on the surface of C_3N_4, the band structures were modified in such a way to reach the equilibrium between the Fermi levels of C_3N_4 and Cu_2O.[34] The negatively charged carriers move to the positive field (n-type C_3N_4) and the positive carriers migrate to the negative field (p-type Cu_2O). In other words, the CB of C_3N_4 behaved as a sink for the photogenerated electrons and subsequently the holes accumulated in the VB of Cu_2O.[35] Presence of rGO facilitated this carrier transport as strongly supported by the PL studies (Figure 5) and thereby increased the photocatalytic activity. The holes were utilized for the conversion of SO_3^{2-} to $SO_3^{\cdot-}$. On the other hand, the photoexcited electrons involved in the reduction of 4-nitrophenol to 4-aminophenol.

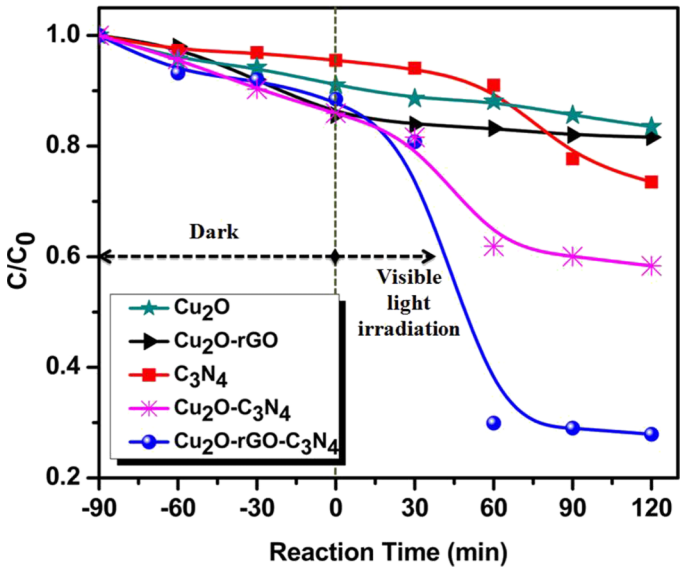

FIG. 6. Photocatalytic reduction of 4-nitrophenol to 4-aminophenol in presence of different photocatalysts.

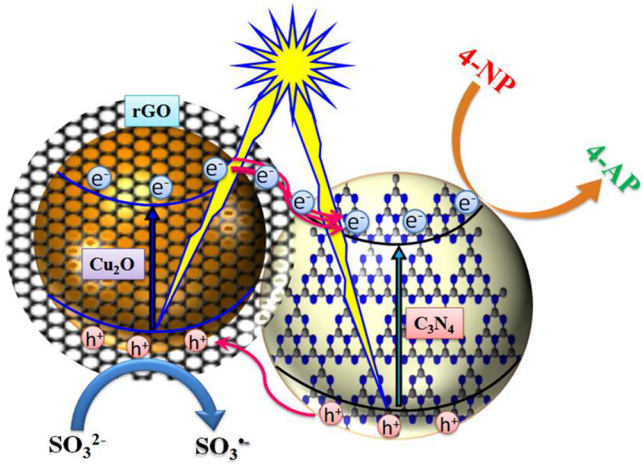

FIG. 7. Plausible mechanism for the photocatalytic reduction of 4-nitrophenol to 4-aminophenol using Cu_2O–rGO–C_3N_4 photocatalyst in presence of sodium sulfite.

In conclusion, rGO wrapped Cu_2O spheres were synthesized and loaded over C_3N_4 photocatalyst. By this synthetic route, the rGO was placed exactly at the interfacial of Cu_2O and C_3N_4 heterojunction and hence the photogenerated carrier migration became very rapid which was authenticated by the PL studies. As a result of this, the photocatalytic reduction ability of Cu_2O–rGO–C_3N_4 was enhanced ~2 fold synergistically as compared with that of the bare C_3N_4 and Cu_2O–rGO photocatalysts. A tentative mechanism was proposed for the reduction of 4-nitrophenol using Cu_2O–rGO–C_3N_4 photocatalyst under visible light irradiation. Photocatalyst recyclability was scrutinized for four times without any measurable loss in its photocatalytic activity.

We acknowledge financial support from the SERB (No. SR/FT/CS-127/2011), DST, New Delhi, India. We also acknowledge Professor B. Viswanathan, National Centre for Catalysis Research, IIT-Chennai for XPS analysis.

[1] P. V. Kamat, Chem. Rev. **93**, 267 (1993).
[2] S. Sakthivel, B. Neppolian, M. V. Shankar, B. Arabindoo, M. Palanichamy, and V. Murugesan, Sol. Energy Mater. Sol. Cells **77**, 65 (2003).
[3] J. Nisar, B. Pathak, and R. Ahuja, Appl. Phys. Lett. **100**, 181903 (2012).
[4] H. Yamashita, M. Harada, J. Misaka, M. Takeuchi, B. Neppolian, and M. Anpo, Catal. Today **84**, 191 (2003).
[5] A. L. Linsebigler, G. Lu, and J. T. Yates, Chem. Rev. **95**, 735 (1995).
[6] M. Suzuki, T. Ito, and Y. Taga, Appl. Phys. Lett. **78**, 3968 (2001).
[7] M. D. H. A. Fuerte, A. J. Maira, A. Martinez-Arias, M. Fernadez-Garcia, J. C. Conesa, and J. Soria, Chem. Commun. **24**, 2718 (2001).
[8] K. Takeuchi, I. Nakamura, O. Matsumoto, S. Sugihara, M. Ando, and T. Ihara, Chem. Lett. **29**, 1354 (2000).
[9] J. C. Yu, L. Zhang, Z. Zheng, and J. Zhao, Chem. Mater. **15**, 2280 (2003).
[10] T. Hirai, K. Suzuki, and I. Komasawa, J. Colloid Interface Sci. **244**, 262 (2001).
[11] D. Chatterjee and A. Mahata, Appl. Catal., B **33**, 119 (2001).
[12] J. Wang, T. Ma, G. Zhang, Z. Zhang, X. Zhang, Y. Jiang, G. Zhao, and P. Zhang, Catal. Commun. **8**, 607 (2007).
[13] X. Wang, K. Maeda, A. Thomas, K. Takanabe, G. Xin, J. M. Carlsson, K. Domen, and M. Antonietti, Nat. Mater. **8**, 76 (2009).
[14] Y. Wang, X. Wang, and M. Antonietti, Angew. Chem., Int. Ed. **51**, 68 (2012).
[15] S. C. Yan, S. B. Lv, Z. S. Li, and Z. G. Zou, Dalton Trans. **39**, 1488 (2010).
[16] S. Yan, Z. Li, and Z. Zou, Langmuir **26**, 3894 (2010).
[17] X. Li, J. Chen, X. Wang, J. Sun, and M. Antonietti, J. Am. Chem. Soc. **133**, 8074 (2011).
[18] L. F. Gou and C. J. Murphy, Nano Lett. **3**, 231 (2003).
[19] Y. Tian, B. Chang, J. Fu, B. Zhou, J. Liu, F. Xi, and X. Dong, J. Solid State Chem. **212**, 1 (2014).
[20] B. Neppolian, A. Bruno, C. L. Bianchi, and M. Ashokkumar, Ultrason. Sonochem. **19**, 9 (2012).
[21] S. G. Babu, R. Vinoth, D. P. Kumar, M. V. Shankar, H.-L. Chou, K. Vinodgopal, and B. Neppolian, Nanoscale **7**, 7849 (2015).
[22] S. G. Babu, R. Vinoth, B. Neppolian, D. D. Dionysiou, and M. Ashokkumar, J. Hazard. Mater. **291**, 83 (2015).
[23] S. G. Babu and R. Karvembu, Ind. Eng. Chem. Res. **50**, 9594 (2011).
[24] S. G. Babu, N. Neelakandeswari, N. Dharmaraj, S. D. Jackson, and R. Karvembu, RSC Adv. **3**, 7774 (2013).
[25] J. Zhu, Y. Wei, W. Chen, Z. Zhao, and A. Thomas, Chem. Commun. **46**, 6965 (2010).

[26] J. S. Lee, K. H. You, and C. B. Park, Adv. Mater. **24**, 1084 (2012).
[27] Y. Zhang, T. Mori, L. Niu, and J. Ye, Energy Environ. Sci. **4**, 4517 (2011).
[28] Y. Bai, T. Yang, Q. Gu, G. Cheng, and R. Zheng, Powder Technol. **227**, 35 (2012).
[29] J. Chen, S. Shen, P. Guo, M. Wang, P. Wu, X. Wang, and L. Guo, Appl. Catal., B **152–153**, 335 (2014).
[30] J. Zhang, J. Sun, K. Maeda, K. Domen, P. Liu, M. Antonietti, X. Fu, and X. Wang, Energy Environ. Sci. **4**, 675 (2011).
[31] A. Paracchino, V. Laporte, K. Sivula, M. Gratzel, and E. Thimsen, Nat. Mater. **10**, 456 (2011).
[32] L. Ge, C. Han, and J. Liu, Appl. Catal., B **108–109**, 100 (2011).
[33] P. Wang, Y. H. Ng, and R. Amal, Nanoscale **5**, 2952 (2013).
[34] Z. Zhang, C. Shao, X. Li, C. Wang, M. Zhang, and Y. Liu, ACS Appl. Mater. Interfaces **2**, 2915 (2010).
[35] J. Cao, X. Li, H. Lin, S. Chen, and X. Fu, J. Hazard. Mater. **239–240**, 316 (2012).
[36] See supplementary material at http://dx.doi.org/10.1063/1.4928286 for detailed experimental procedures for the preparation of materials, instrumental parameters and some of the results.

Reduced graphene oxide wrapped Cu_2O supported on C_3N_4: An efficient visible light responsive semiconductor photocatalyst

S. Ganesh Babu,[1] R. Vinoth,[1] P. Surya Narayana,[1] Detlef Bahnemann,[2] and B. Neppolian[1,*]

[1]*SRM Research Institute, SRM University, Kattankulathur, Chennai 603203, India*
[2]*Institute of Technical Chemistry, Leibniz University of Hannover, D-30167, Hannover, Germany*

Supplemental Material

Graphite powder (synthetic, conducting grade, 325 mesh, 99.9995%) was obtained from Alfa Aesar. Cupric acetate ($Cu(CH_3COO)_2 \cdot H_2O$) was procured from Loba Chemie Pvt. Ltd. 3-aminopropyltriethoxysilane (APTES), glucose ($C_6H_{12}O_6$), polyvinylpyrrolidone (PVP, K-30) and 4-nitrophenol were purchased from Sigma Aldrich. N,N-dimethylformamide (DMF), isopropanol, $NaNO_3$, $KMnO_4$, H_2SO_4 and H_2O_2 were purchased from Rankem, India. Milli-Q ultrapure water through Q-POD (Merck Millipore system, conductivity 18.2 MΩ) was used in all experiments. An ultrasonic bath (WENSAR, 40 kHz and 25 L capacity, India) was used for the homogenous dispersion of graphene oxide (GO) in water.

Graphene oxide (GO) was prepared from graphite using $NaNO_3$, $KMnO_4$, H_2SO_4 and H_2O_2 by following modified Hummer's method.[1] Cu_2O spheres were prepared by following the literature procedure.[2] In detail, 8 mmol of $Cu(CH_3COO)_2 \cdot H_2O$ and 6 mmol of PVP(K-30) were dissolved in DMF (120 mL). 8.5 mmol of Glucose was added to the above solution as a reducing agent for the reduction of Cu^{2+} to Cu^{+}. The solution was stirred vigorously for for 30 min at 27 ºC. Then the whole mixture was heated to 85 ºC and stirred for 3 min at this temperature and thereby the color of the mixture became tan. The final product was centrifuged, washed with alcohol and water several times to get pure Cu_2O spheres.

The as-prepared Cu_2O spheres were surface modified using APTES. Typically, 0.1 g of Cu_2O spheres was homogeneously dispersed in 9.9 mL of isopropanol by ultrasonication. Then 0.1 mL of APTES was added into the above mixture and stirred at 27 ºC for 24 h. The final solution was centrifuged and washed several times with ethanol.

For the preparation of 1% rGO loaded Cu_2O spheres, 1 mg of GO was ultrasonicated in de-ionized water (5 mL) for 1 h. To this solution, 0.1 g of APTES surface modified Cu_2O spheres were added and stirred for 3 h at 27 ºC. Then the solution was centrifuged, washed with water and

dried at room temperature. For the reduction of GO to reduced GO (rGO), the final powder sample was calcinated at 350 ºC with the increasing temperature rate of 2 ºC/min under a flowing N_2 atmosphere. rGO wrapping was restricted to 1% mainly because higher amount of rGO loading covers the whole Cu_2O spheres (make the sample more black) and prevent the penetration of light to fall on Cu_2O spheres.

Pyrolysis synthetic route was followed for the preparation of C_3N_4.[3] 3 g of melamine was crushed completely in a pastel-mortar for 30 min and then transferred into a crucible which covered semi-closely with a lid to prevent sublimation of melamine, heated in a muffle furnace at 500 ºC with the heating rate of 20 ºC/min that was kept at this temperature for 4 h. Then the temperature was raised further to 520 ºC at the rate of 10 ºC/min, and kept at this temperature for 2 h. The sample was allowed to cool naturally to room temperature. The yellow polymer that obtained by this pyrolysis were ground into powder.

Cu_2O-rGO-C_3N_4 photocatalysts were prepared by following the wet impregnation technique. The required amount of rGO wrapped Cu_2O spheres (5, 10, 15 and 20%) were mixed with C_3N_4 that dispersed in water. The solution was ultrasonicated for 5 min for the homogenous mixing and then stirred at 80 ºC to evaporate water completely.

The crystal structure of C_3N_4, Cu_2O, Cu_2O-rGO and Cu_2O-rGO-C_3N_4 photocatalysts were studied using PANaltical X'pert powder diffractometer (XRD) recorded with Cu Kα radiation. UV-vis DRS measurements were carried out over Specord-200 plus UV-vis spectrophotometer, Germany in DRS mode. The hierarchy, surface morphology and elemental weight percentage were determined by FESEM and EDS analysis, respectively (FEI Quanta FEG 200 HR-SEM which operated at 20 kV). TEM analysis was performed using a JEM-2100 JEOL (Japan) with an accelerating voltage of 120 kV. Photoluminescence (PL) studies were performed using Jasco FP-

8300 spectrophotometer in the wavelength range, 300–800 nm using an excitation wavelength of 280 nm. Fourier Transform Infrared (FT-IR) spectra were recorded using Perkin-Elmer-USA.

Photocatalytic reduction of 4-nitrophenol was performed in a quartz photoreactor system containing 15 ppm of 4-nitrophenol (100 mL), Na_2SO_3 (200 mg, 0.025 M) and 50 mg of the photocatalyst powder. The mixture was stirred under dark for 90 min at 400 rpm to reach adsorption-desorption equilibrium. Then, the suspension was irradiated with an external light source (150 W tungsten lamp) which emitting wavelength (λ) of > 420 nm. The photocatalytic reduction of 4-nitrophenol was estimated using Specord-200 plus UV-vis spectrophotometer by following the disappearance of the absorption band at 400 nm.

Figure S1 shows the absorbance spectroscopic results of bare C_3N_4, bare Cu_2O and Cu_2O-rGO-C_3N_4, and also gives the clear picture of Tauc plot of C_3N_4, Cu_2O and Cu_2O-rGO-C_3N_4 composites.

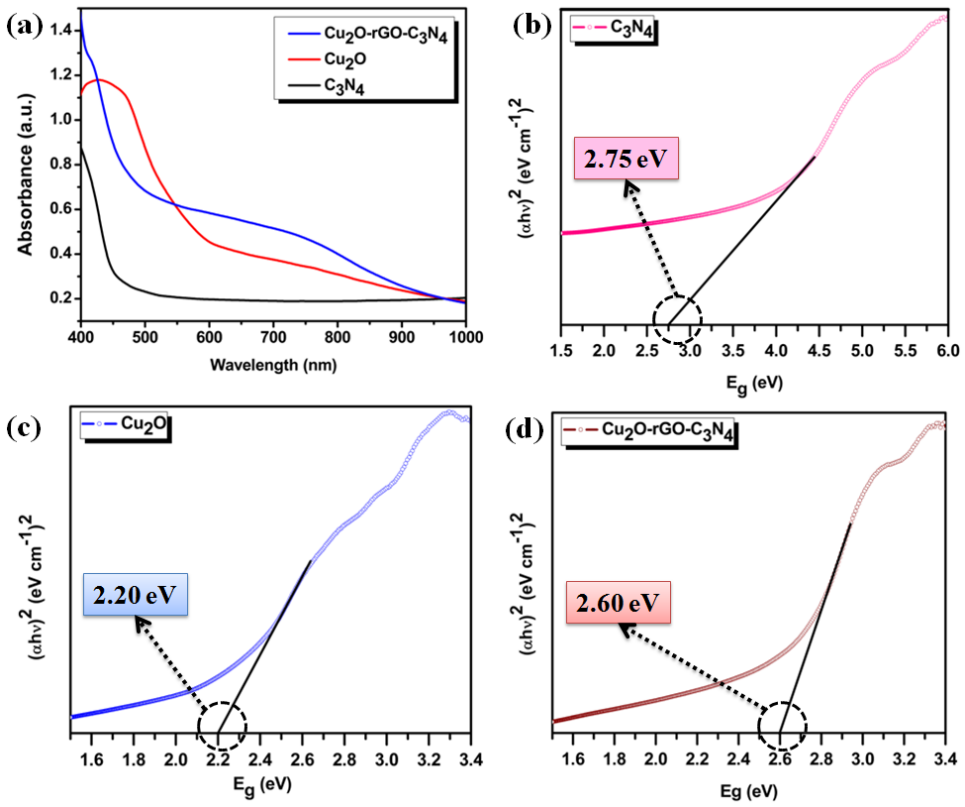

Figure S1. (a) Absorbance spectroscopic results of bare C_3N_4, bare Cu_2O and Cu_2O-rGO-C_3N_4, and Tauc plot of (b) C_3N_4, (c) Cu_2O and (d) Cu_2O-rGO-C_3N_4 composite.

Figure S2 depicts the FTIR spectra of Cu_2O, C_3N_4, APTES Cu_2O, Cu_2O-rGO and Cu_2O-rGO-C_3N_4 photocatalysts. Pure C_3N_4 showed a characteristic band centred at 807 cm^{-1} which might be due to the out-of-plane bending vibration of the triazine rings. The bands in the region of 800-1250 cm^{-1} were allocated to the typical stretching modes of C-N heterocylces. FTIR spectra of C_3N_4 based photocatalysts exhibited peaks at 806, 883 and 1242 cm^{-1} which were assigned to the C-N stretching. Similarly, the Cu-O stretching band was observed around 627 cm^{-1} in pure Cu_2O, APTES modified Cu_2O, Cu_2O-rGO photocatalysts. Nevertheless, the intensity of Cu-O stretching band was comparatively less in Cu_2O-C_3N_4-rGO photocatalyst as compared to that of the other Cu_2O loaded photocatalysts (pure Cu_2O, APTES modified Cu_2O, Cu_2O-rGO photocatalysts) which was exactly owing to the lesser loading of Cu_2O in Cu_2O-C_3N_4-rGO photocatalyst. The

oxygen rich functional groups especially the -C-O, -C=O and -C-O-C- bonds bending and stretching frequencies of rGO were observed at around 1220 to 1670 cm^{-1}. Likewise the O-H stretching band of hydroxyl group present in the rGO was renowned at around 3450 cm^{-1}.

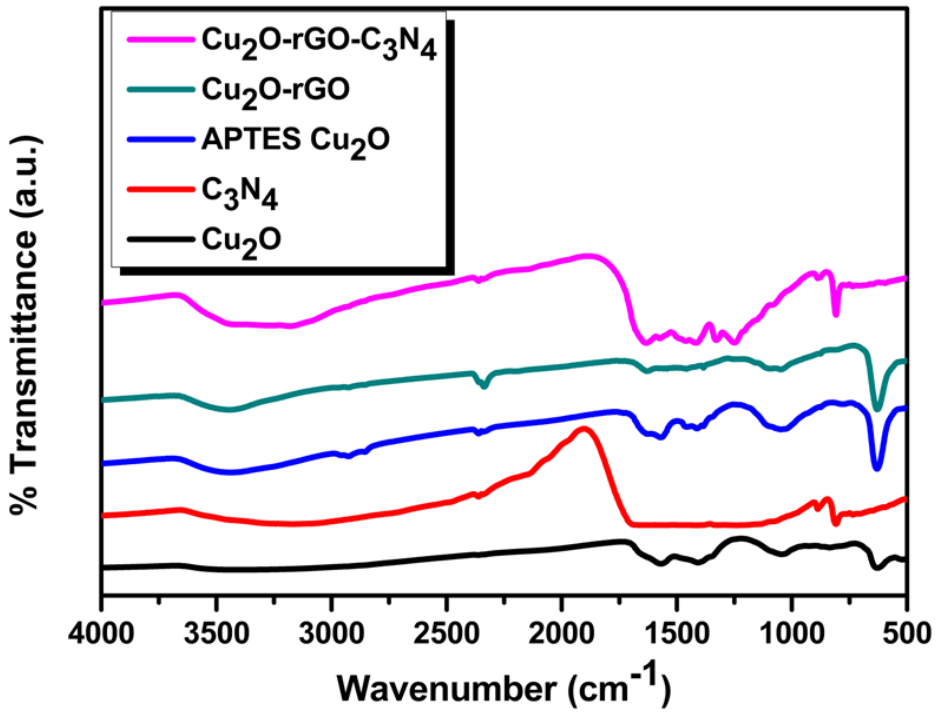

Figure S2. FTIR spectra of Cu_2O, C_3N_4, APTES Cu_2O, Cu_2O-rGO and Cu_2O-rGO-C_3N_4 photocatalysts.

Figure S3 shows the TEM image of Cu_2O-rGO-C_3N_4 photocatalyst. The TEM image clearly confirmed the presence of Cu_2O spheres. Moreover, a thin layer of rGO was wrapped with rGO which was inferred from TEM image. This rGO wrapped Cu_2O spheres were firmly anchored on the surface of C_3N_4. Furthermore, the rGO layer was placed exactly at the interface of Cu_2O and C_3N_4 interfacial heterojunction. Very interestingly, the porous nature of the C3N4 photocatlyst was also evidenced from the TEM image. This particular property of the photocatlytic material appreciably increased the adsorption of 4-nitrophenol on the surface and hence the photoreduction process was enhanced significantly.

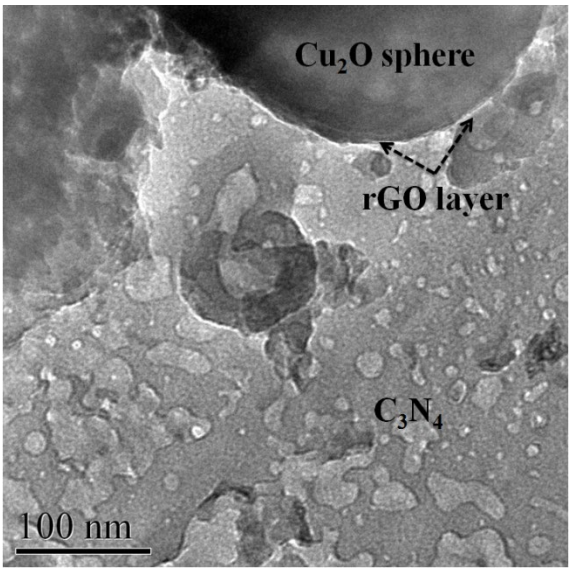

Figure S3. TEM image of Cu_2O-rGO-C_3N_4 photocatalyst.

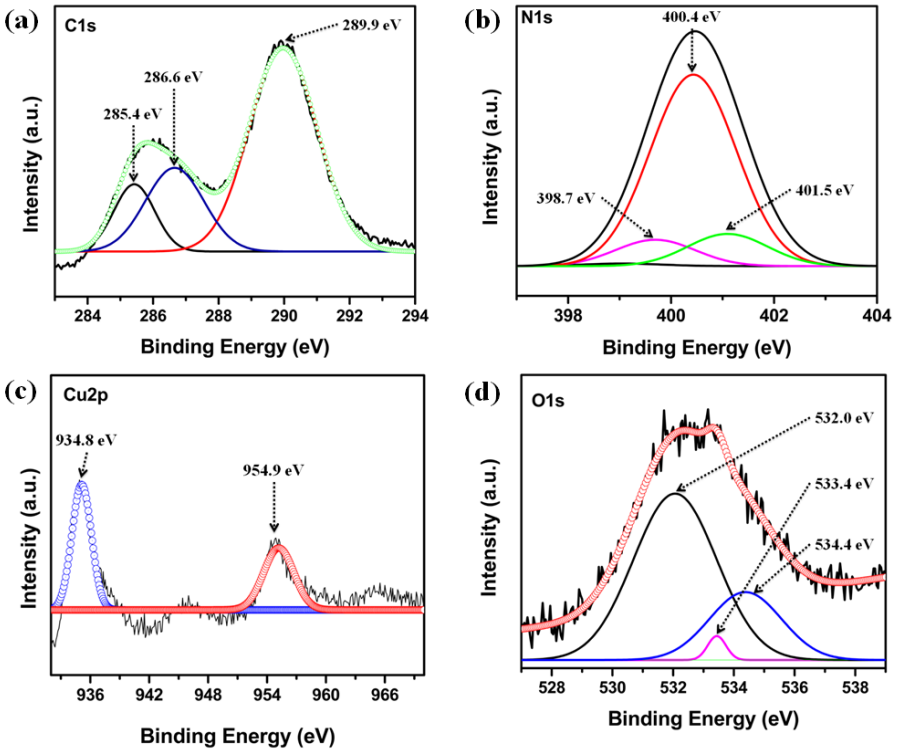

Figure S4. XPS spectra of the Cu_2O-rGO-C_3N_4 photocatalyst: (a) high resolution C1s spectrum, (b) high resolution N1s spectrum, (c) high resolution Cu2p spectrum and (d) high resolution O1s spectrum.

The chemical oxidation states of Cu_2O-rGO-C_3N_4 composites were found using XPS analysis. Figure S4 depicts the high resolution C1s, N1s, Cu2p and O1s spectra of Cu_2O-rGO-C_3N_4 photocatalyst. Figure S4(a) shows the high resolution C1s spectra and can be deconvoluted into three peaks at 285.4, 286.6 and 289.9 eV, which are mainly assigned to the sp^2 bonded carbon atoms such as carbon-carbon double bond (C=C), carbonyl (C=O) groups and carbon-nitrogen double bond (C=N), respectively.[4] Figure S4(b) clearly shows that the N1s spectra can be deconvoluted into three peaks located at 398.7, 400.4 and 401.5 eV which are attributed to the C–N=C, N–$(C)_3$ and C–N–H groups, respectively.[5] The existence of secondary C–N–H groups clearly indicated the formation of chemical bonds between rGO and C_3N_4.[6] Figure S4(c) shows the high resolution Cu2p spectra that can be fitted into two major peaks centered at 934.8 and 954.9 eV which was mainly attributed to Cu^+ state of Cu2p3/2 and Cu2p1/2, respectively. This result clearly confirmed the existence of Cu_2O in the composites.[7] Furthermore, a small satellite peaks with higher binding energy compared to that of Cu2p3/2 and Cu2p1/2 were observed that might be owing to the over oxidation of Cu^+ ions on the surface of the photocatalyst.[8] Generally the Cu_2O based photocatalysts are unstable because of the easy oxidation of Cu_2O to CuO. Nevertheless in the present system the Cu_2O spheres are relatively stable, especially the rGO layer which wrapped on the surface of the Cu_2O spheres prevent the over oxidation and make the photocatalyst more stable. Likewise, the deconvolution of O1s into three peaks are appeared in 532, 533.4 and 534.4 eV which were ascribed to epoxy or hydroxyl, ester and carboxylic groups.[9]

The experimental results suggested that Cu_2O-rGO-C_3N_4 composite rapidly involved in the reduction of 4-nitrophenol to 4-aminophenol and thereby it is indispensable to optimize the loading of rGO wrapped Cu_2O to C_3N_4. For this purpose different weight percentage of Cu_2O-rGO (0, 5, 10, 15 and 20 wt%) loaded C_3N_4 was prepared and the photocatalytic activity was tested against

the reduction of 4-nitrophenol. Figure S5 shows the respective results. Amongst the different weight percentage Cu_2O-rGO loaded catalysts, the 15% Cu_2O-rGO loaded C_3N_4 exhibited the maximum photoreduction activity. Further increase of Cu_2O-rGO loading has no remarkable influence on the photocatalytic reduction of 4-nitrophenol to 4-aminophenol. The possible reason could be that above the monolayer dispersion, agglomeration of Cu_2O-rGO on the C_3N_4 surface may occur while increasing the Cu_2O-rGO loading which resulted in ineffective photocatalytic ability besides the light screening effect. Hence the weight percentage loading of Cu_2O-rGO was optimized to be 15% and the same catalyst was used for the durability studies.

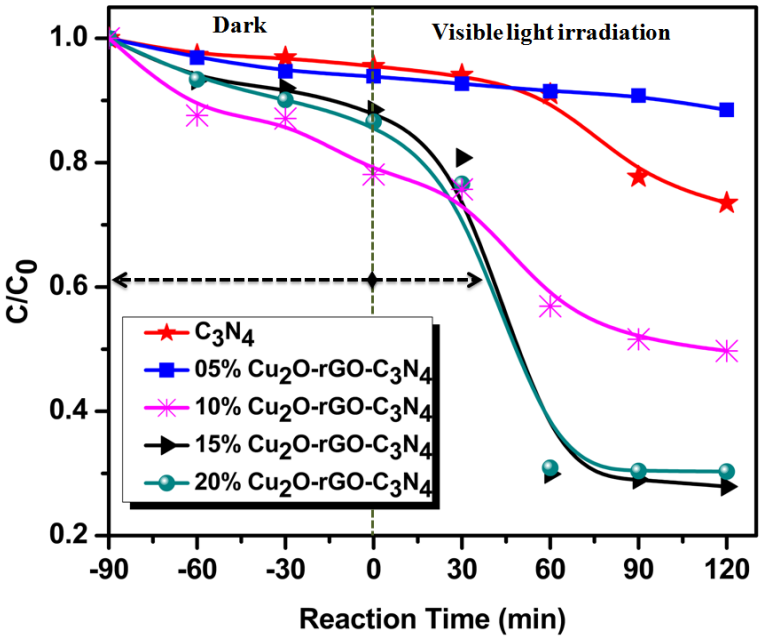

Figure S5. Optimization of Cu_2O-rGO loading in C_3N_4 for the photoreduction of 4-nitrophenol to 4-aminophenol.

It is paramount important to optimize the rGO content in the final Cu_2O-rGO-C_3N_4 composite photocatalyst. For this purpose, different weight percentage rGO (0, 0.5, 1.0, 1.5 and 2.0 wt%) wrapped Cu_2O was initially prepared and subsequently the as synthesized Cu_2O-rGO

was loaded on C_3N_4. The photocatalytic reduction of 4-nitrophenol to 4-aminophenol was tested by using the different weight percentage rGO loaded photocatalysts. Figure S6 implies that the initial loading of rGO increased the photocatalytic performance and it reached a maximum with 1.0 wt% rGO loaded photocatalyst. But further increase of rGO loading (1.5 and 2.0 wt%) decreased significantly the photocatalytic activity. This could be possibly due to the fact that the higher loading of rGO made the sample black and thereby prevent the interaction of photon with Cu_2O which resulted in lesser generation of electron-hole pairs in Cu_2O spheres.

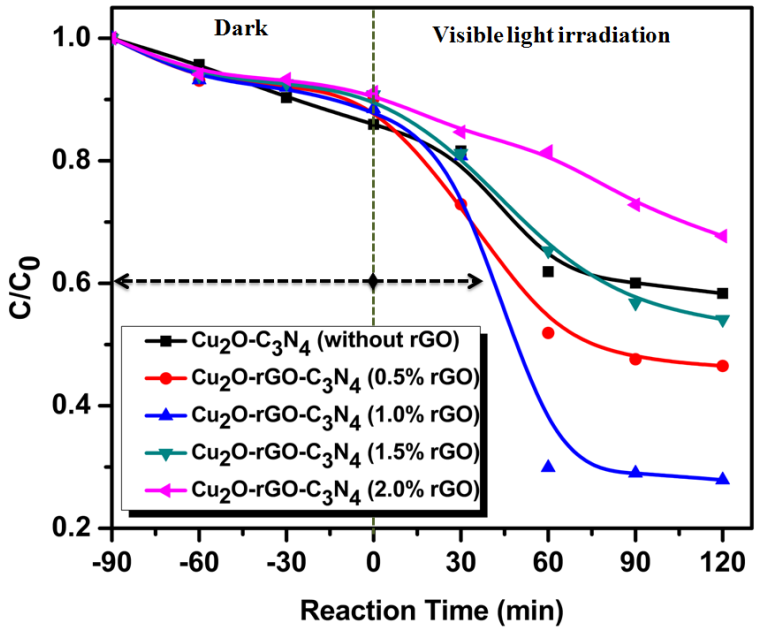

Figure S6. Optimization of rGO loading in Cu_2O-C_3N_4 for the photoreduction of 4-nitrophenol to 4-aminophenol.

Durability of any heterogeneous catalyst is paramount important, especially for the economic and environmental points of view. Therefore durability of the as-prepared Cu_2O-rGO-C_3N_4 photocatalyst was tested with 4-nitrophenol. The reduction efficiency of the recycled photocatalyst was monitored using UV-vis spectrophotometer. Figure S7 shows the corresponding

reusability results. The results implied that this photocatalyst can be reused for four cycles without losing its catalytic activity, which is an advantage of using the catalysts for industrial applications.

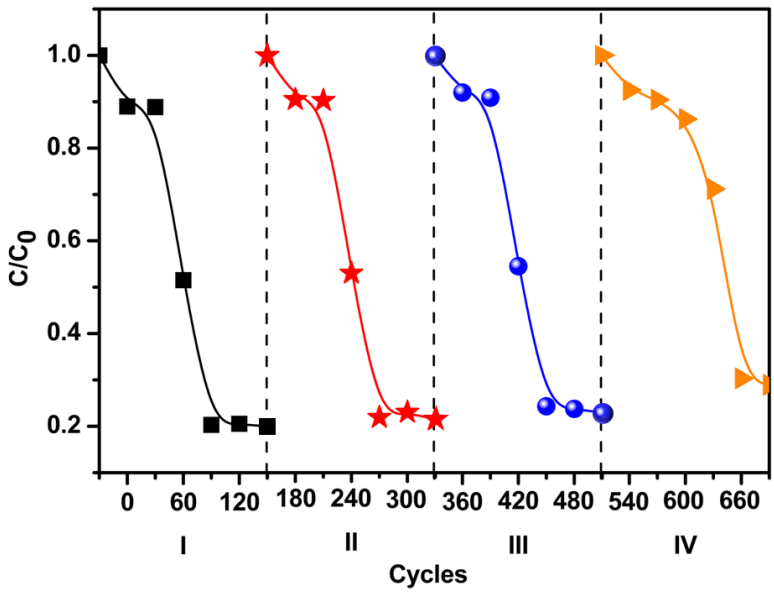

Figure S7. Durability test results of Cu_2O-rGO-C_3N_4 for the photoreduction of 4-nitrophenol to 4-aminophenol.

[1] W. S. Hummers, and R. E. Offeman, J. Am. Chem. Soc. **80**, 1339 (1958).

[2] L.J. Cote, F. Kim, and J. Huang, J. Am. Chem. Soc. **131**, 1043 (2009).

[3] Y. –T. Xu, Y. Guo, C. Li, X. –Y. Zhou, M. C. Tucker, X. –Z. Fu, R. Sun, and C. –P. Wong, Nano Energy **11**, 38 (2015). G. Xin, and Y. Meng, J. Chem. **2013**, 5 (2013).

[4] M. Gopiraman, S. G. Babu, Z. Khatri, K. Wei, E. Morinobu, R. Karvembu, and I. S. Kim, Catal. Sci. Tech. **3**, 1485 (2013).

[5] B. Peng, S. Zhang, S. Yang, H. Wang, H. Yu, S. Zhang, and F. Peng, Mater. Res. Bull. **56**, 19 (2014).

[6] Y. Fu, J. Zhu, C. Hu, X. Wu, and X. Wang, Nanoscale **6**, 12555 (2014).

[7] S. G. Babu, R. Vinoth, D. P. Kumar, M. V. Shankar, H. –L. Chou, K. Vinodgopal and B. Neppolian, Nanoscale 7, 7849 (2015).

[8] S. G. Babu, R. Vinoth, B. Neppolian, D. D. Dionysiou, and M. Ashokkumar, J. Hazard. Mater. **291**, 83 (2015).

[9] M. Gopiraman, S. G. Babu, Z. Khatri, W. Kai, Y. A. Kim, M. Endo, R. Karvembu, and Ick Soo Kim, J. Phy. Chem. C **117**, 23582 (2013).

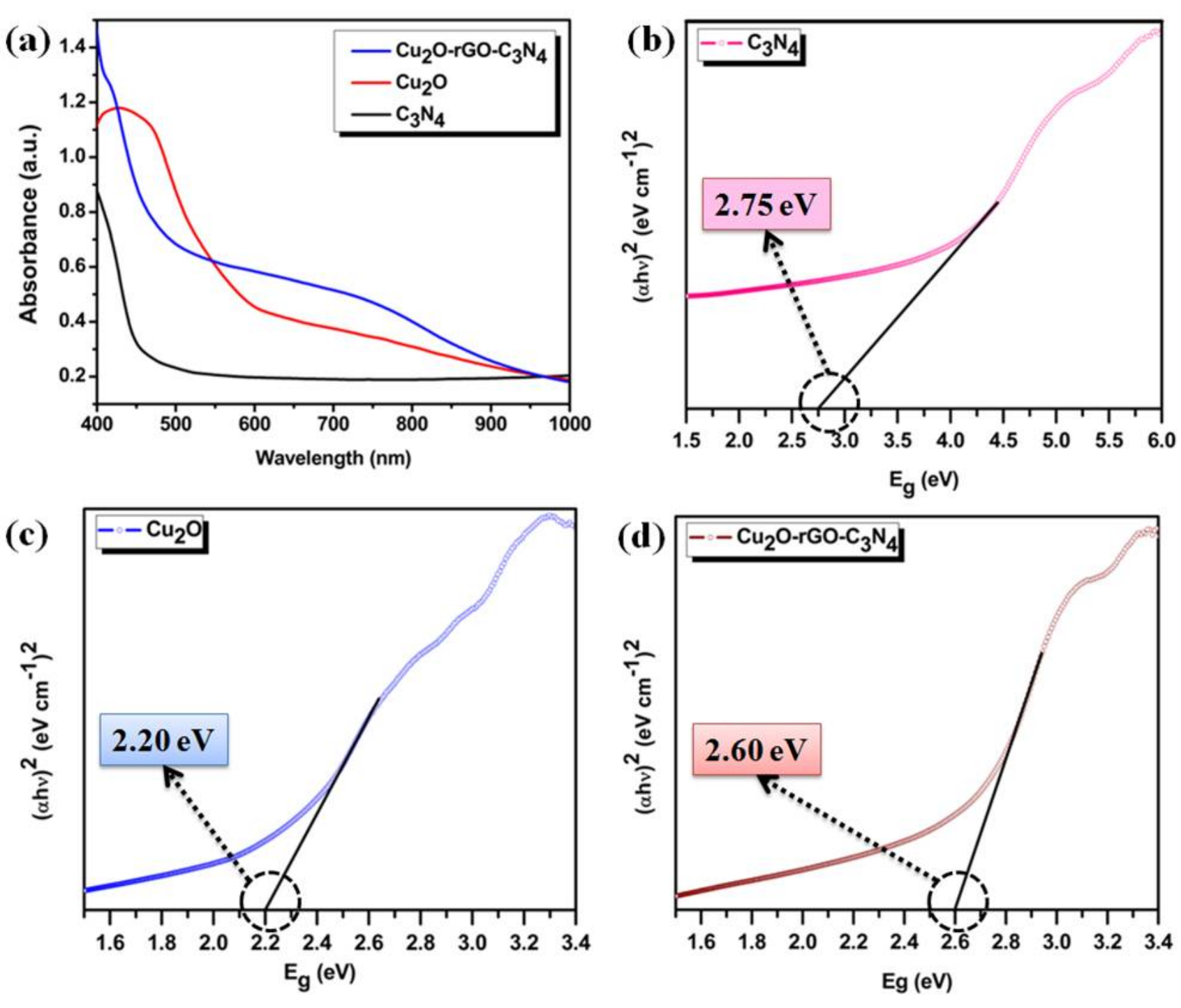
(a)
Cu2O-rGO-C3N4
Cu2O
C3N4
Absorbance (a.u.)
Wavelength (nm)
(b)
C3N4
2.75 eV
(αhν)2 (eV cm-1)2
Eg (eV)
(c)
Cu2O
2.20 eV
(αhν)2 (eV cm-1)2
Eg (eV)
(d)
Cu2O-rGO-C3N4
2.60 eV
(αhν)2 (eV cm-1)2
Eg (eV)

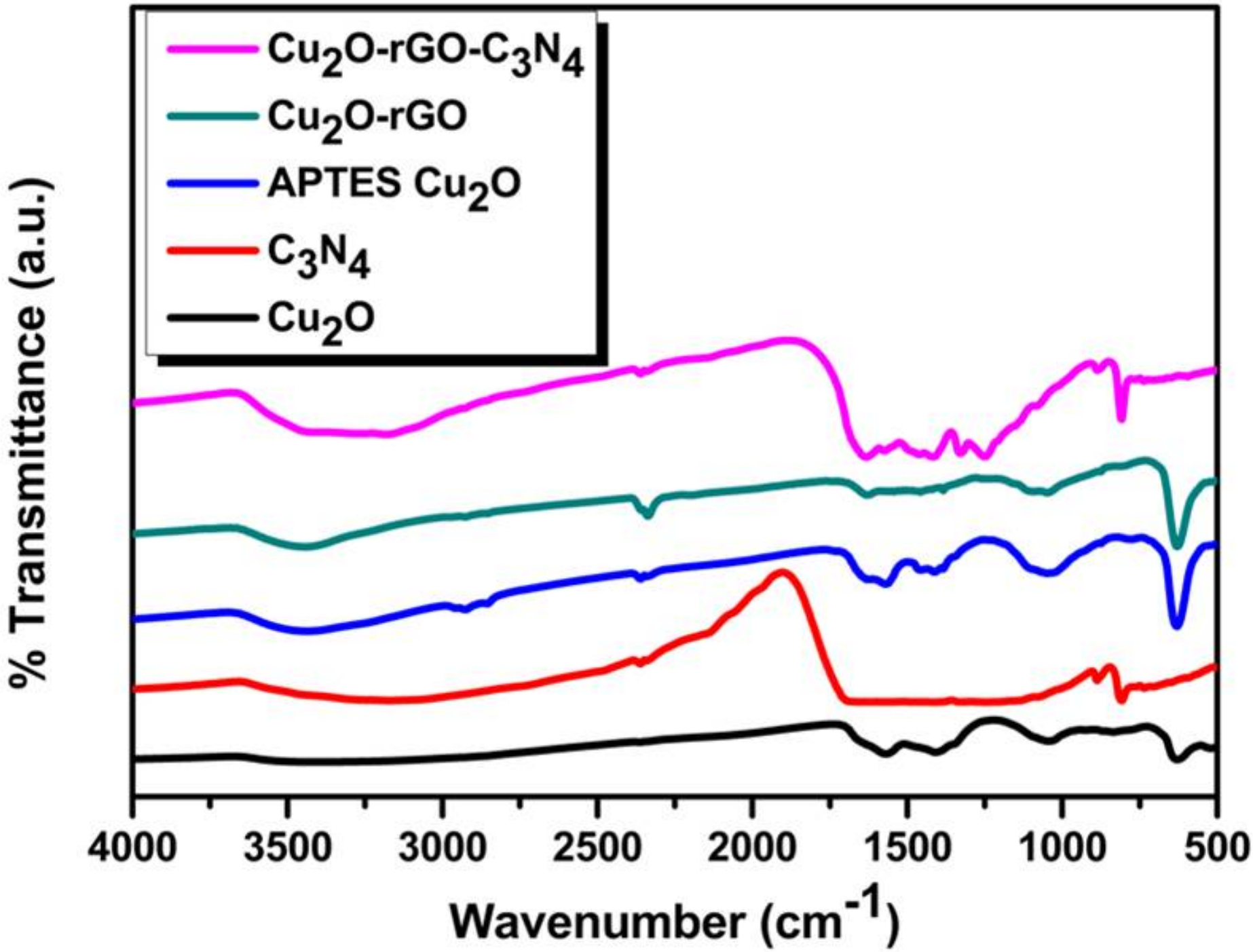
Cu2O-rGO-C3N4
Cu2O-rGO
APTES Cu2O
C3N4
Cu2O
% Transmittance (a.u.)
4000
3500
3000
2500
2000
1500
1000
500
Wavenumber (cm-1)


Cu_2O sphere
rGO layer
C_3N_4
100 nm

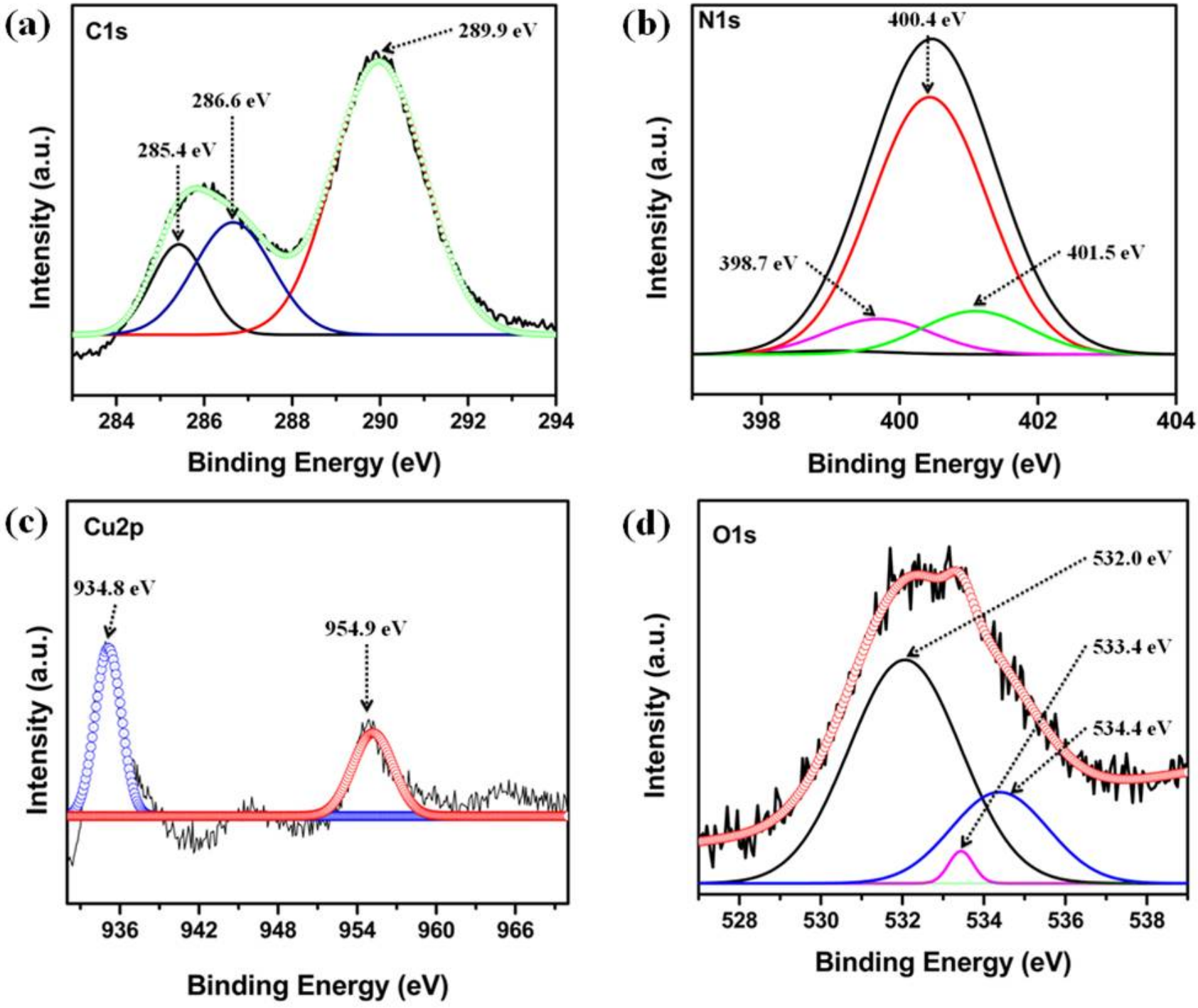
(a)
C1s
289.9 eV
286.6 eV
285.4 eV
Intensity (a.u.)
284
286
288
290
292
294
Binding Energy (eV)
(b)
N1s
400.4 eV
398.7 eV
401.5 eV
Intensity (a.u.)
398
400
402
404
Binding Energy (eV)
(c)
Cu2p
934.8 eV
954.9 eV
Intensity (a.u.)
936
942
948
954
960
966
Binding Energy (eV)
(d)
O1s
532.0 eV
533.4 eV
534.4 eV
Intensity (a.u.)
528
530
532
534
536
538
Binding Energy (eV)

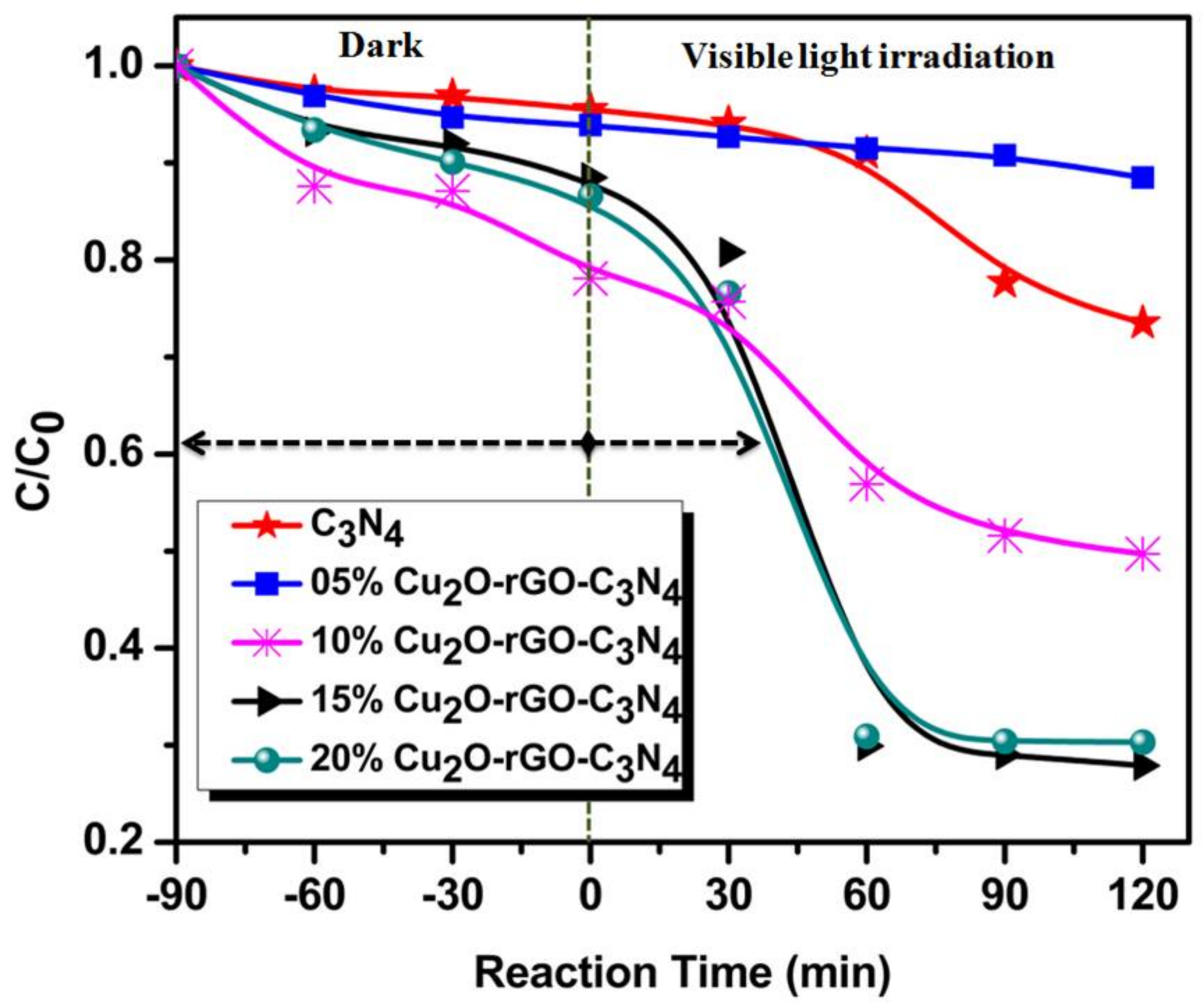
Dark
Visible light irradiation
1.0
0.8
0.6
0.4
0.2
C/C0
-90
-60
-30
0
30
60
90
120
Reaction Time (min)
C3N4
05% Cu2O-rGO-C3N4
10% Cu2O-rGO-C3N4
15% Cu2O-rGO-C3N4
20% Cu2O-rGO-C3N4

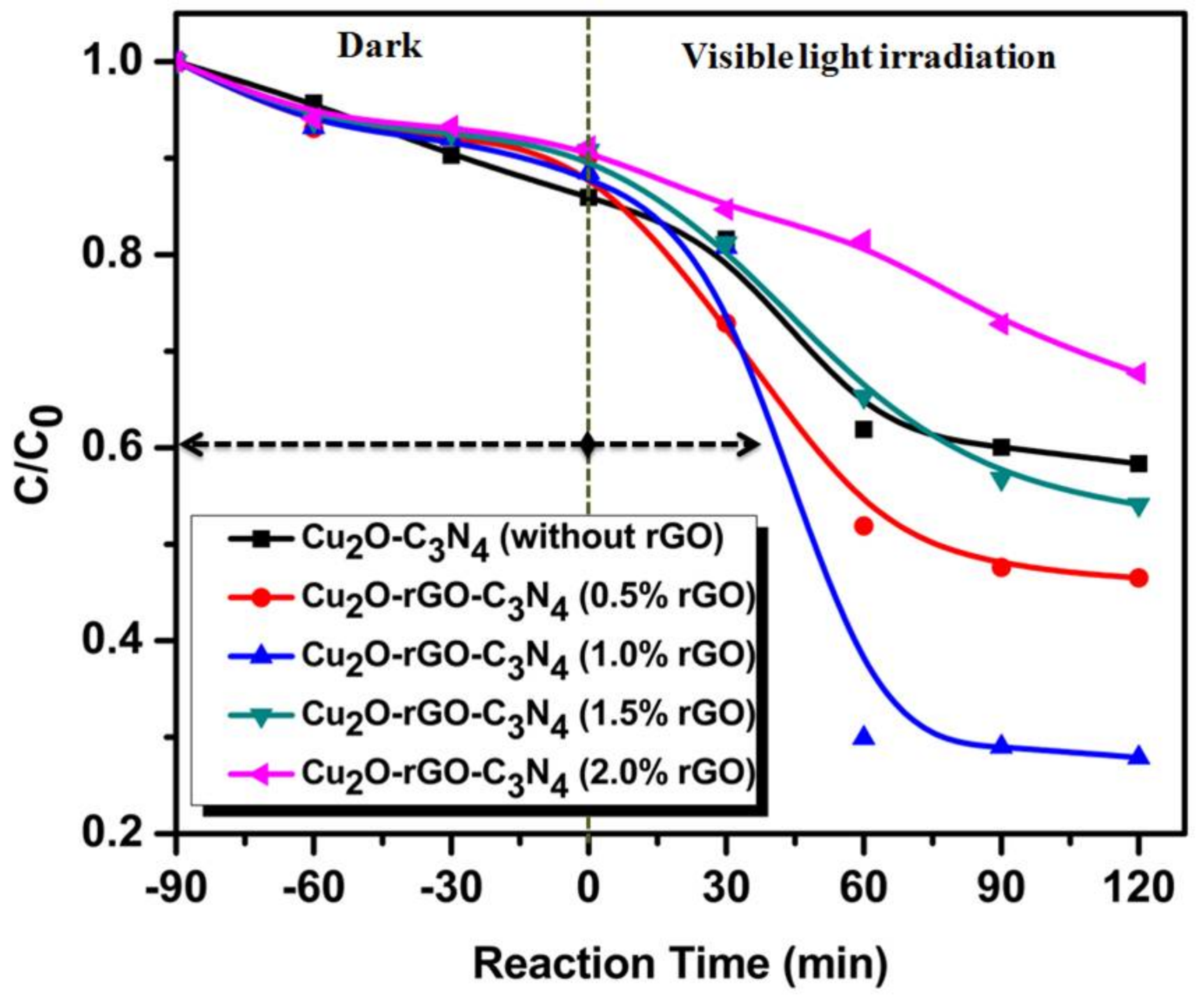
Dark
Visible light irradiation
1.0
0.8
0.6
0.4
0.2
C/C0
-90
-60
-30
0
30
60
90
120
Reaction Time (min)
Cu2O-C3N4 (without rGO)
Cu2O-rGO-C3N4 (0.5% rGO)
Cu2O-rGO-C3N4 (1.0% rGO)
Cu2O-rGO-C3N4 (1.5% rGO)
Cu2O-rGO-C3N4 (2.0% rGO)

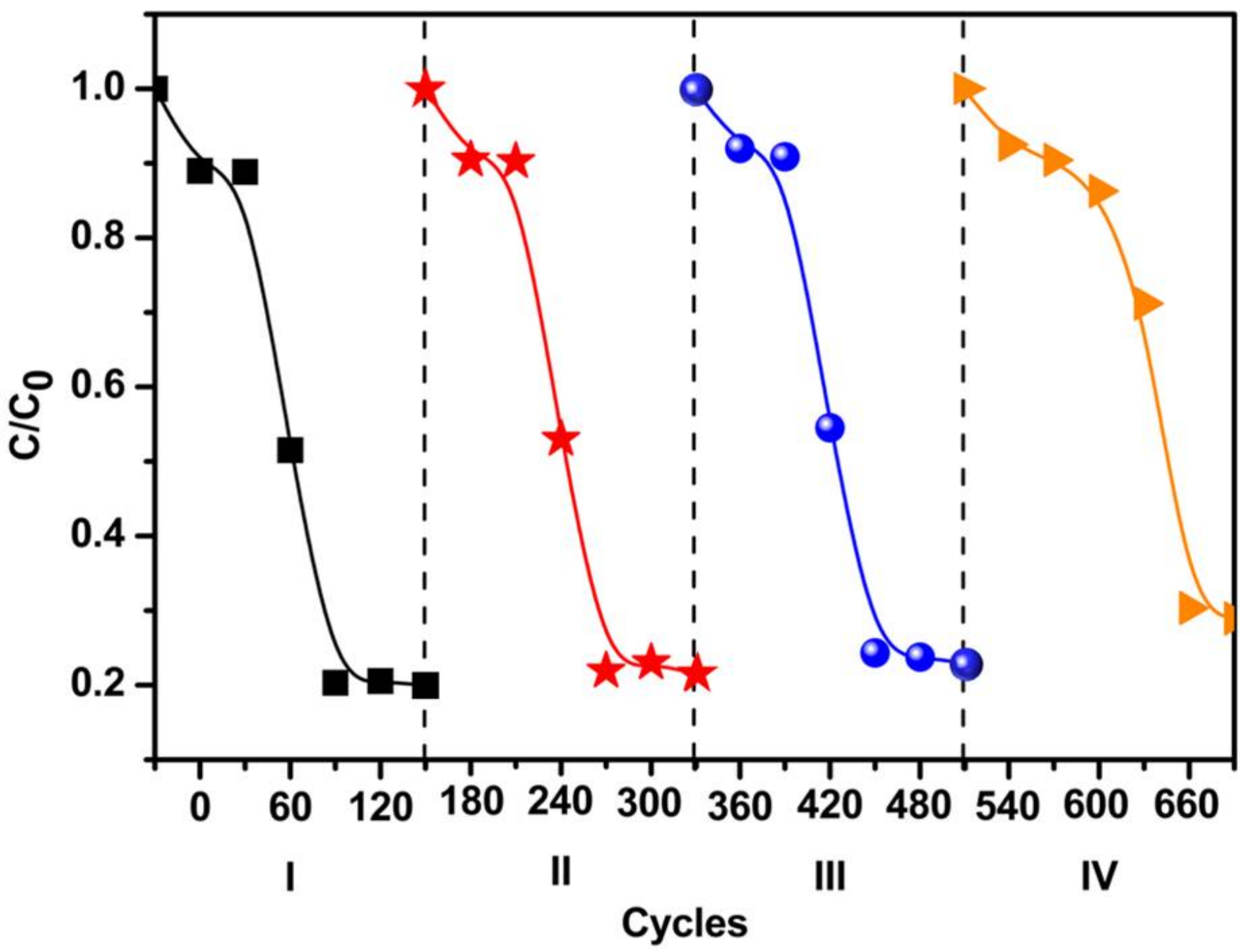
1.0
0.8
0.6
0.4
0.2
C/C0
0
60
120
180
240
300
360
420
480
540
600
660
I
II
III
IV
Cycles